J Prosthodont Res. 2022; 66(4): 589–599

OPEN ACCESS

Journal of Prosthodontic Research

Original article

Influence of molding angle on the trueness and defects of removable partial denture frameworks fabricated by selective laser melting

Hiro Kobayashi [a], Akinori Tasaka [a], Shizuo Higuchi [b], Shuichiro Yamashita [a,*]

[a] Department of Removable Partial Prosthodontics, Tokyo Dental College, Tokyo, Japan

[b] Department of Oral Health Engineering, Faculty of Health Sciences, Graduate School of Oral Health Sciences, Osaka Dental University, Osaka, Japan

Abstract

Purpose: To examine the effect of molding angle on the trueness and defects associated with removable partial denture (RPD) frameworks fabricated by selective laser melting (SLM).

Methods: A plaster model of a partially edentulous mandibular arch classified as Kennedy class II modification 1 was used. After obtaining the 3D data of the model (design data), a framework was designed using CAD software. Based on the design data, three different molding angle conditions (0°, 45°, and −45°) were set in the CAM software. The frameworks were fabricated by SLM under each condition, and 3D data were captured (fabrication data). The design and fabrication data were superimposed using 3D inspection software to verify the shape errors. The number of support structures was then measured. To examine the internal defects, micro-computed tomography (μCT) was performed for void analysis. Surface roughness was measured using a laser microscope.

Results: The overall shape errors of the RPD framework were smaller under the 0° condition compared with the others, and the largest number of support structures was observed at 0°. Many internal defects were observed in the large components of the framework at 45° and −45°. The surface roughness was the smallest at −45°.

Conclusion: The trueness and defects associated with the RPD frameworks were affected by the difference in the SLM molding angle.

Keywords: Removable partial dentures, Metal framework, CAD/CAM, Selective laser melting

Received 14 July 2021, Accepted 16 November 2021, Available online 29 December 2021

1. Introduction

Digital technology is currently widely used in the medical field and has spread widely throughout the dental field over the past few decades[1–4]. It has attracted attention not only in clinical practice, but also in education and research[5,6]. Particularly in the field of prosthodontics, digital technology has been recognized in recent years as indispensable. In particular, the practical application of CAD/CAM technology in prosthodontic clinical practice has brought great benefits, such as time savings and the simplification of tasks that have been performed analogically in the past[7–10].

Among the CAD/CAM technologies, selective laser melting (SLM), a method of layering metal powders with a laser, has enabled the fabrication of frameworks for removable partial dentures (RPDs) [11]. It has been reported that the alloys used for SLM have more precise and superior mechanical and fatigue properties than casting alloys[12]. In addition, it has been reported that the frameworks fabricated by SLM have higher trueness than those fabricated with the conventional casting method[13]. Furthermore, SLM has the advantage of simplifying the work and greatly reducing the risks of fabrication and human errors among dental technicians[7,14]. However, even when frameworks are fabricated by SLM, many operations, such as CAD/CAM software operation, removal of support structure, and polishing of frameworks, still depend on the ability of technicians[15]. Therefore, the fabrication of the RPD framework cannot be fully automated, even using SLM.

In RPD frameworks, the fitness of the components is important[16,17]. Tasaka et al.[7] reported that large deformations occurred in the center of the lingual bar of a framework fabricated by SLM. Therefore, to improve such large deformations caused by SLM, it is necessary to study the appropriate manufacturing conditions. Kanazawa et al.[18] reported that the fitness of the framework of a complete denture fabricated by SLM was affected by the molding angle of the object relative to the platform of the SLM machine. Conversely, it has been reported that titanium frameworks of mandibular bilateral free end RPDs fabricated by SLM showed better fitness with the frameworks set horizontally with respect to the platform, compared with those of groups set at 45° or vertically with respect to the platform[19]. However, no clear evidence has been presented regarding the ideal molding angle, which is currently set according

DOI: https://doi.org/10.2186/jpr.JPR_D_21_00175

***Corresponding author:** Shuichiro Yamashita, Department of Removable Partial Prosthodontics, Tokyo Dental College, 2-9-18 Kandamisakicho, Chiyoda-ku, Tokyo 101-0061, Japan.

E-mail address: syamashita@tdc.ac.jp

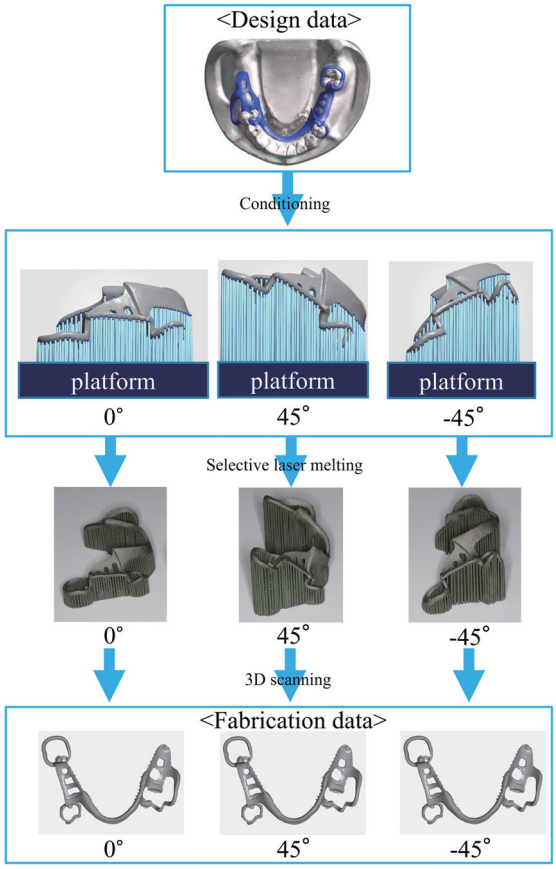

Fig. 1. Flowchart from design data to fabrication data.

to the experience and intuition of the dental technician[20].

It has been reported that the molding angle affects the properties of metals[21]. Because it has been reported that the pattern of internal defects is affected by the molding conditions[22], the molding angle could also be involved in the generation of these internal defects. It has also been reported that the surface roughness using SLM increases compared with that using conventional methods[23,24]. However, few studies have been conducted regarding how the molding angle affects the surface roughness of the framework.

In this study, we hypothesized that the trueness, internal defects, and surface roughness of the framework would differ depending on the SLM molding angle. Verifying this hypothesis could be expected to promote the production of high-quality frameworks with high trueness and few defects.

Given this background, the purpose of this study was to examine the effect of the molding angle on the trueness, internal defects, and surface roughness of RPD frameworks fabricated using SLM.

2. Materials and Methods

2.1. Production of samples

2.1.1. Design data

For the design of the RPD in this study, Stewart's clinical removable partial prosthodontics[25] and McCracken's removable

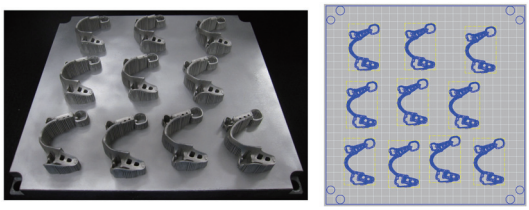

Fig. 2. Image of the placement of the RPD framework. Left: completed frameworks on the platform, right: Image of the placement of RPD frameworks using CAM software.

partial prosthodontics[26] were used as guidelines. A plaster model (MIS3004-L-PL-28; NISSIN, Tokyo, Japan) of a partially edentulous mandibular arch (Kennedy class II modification 1) was used as the simulation model (**Fig. 1**). In this model, rest seats were formed distally on #34 (FDI two-digit system), mesially on #37, and mesially on #45, and guide planes were formed distally on #34, mesially on #37, and distally on #45. After obtaining the 3D data (design data) of the plaster model using a 3D scanner (Smart Big; Open Technologies, Brescia, Italy), an RPD framework was designed using CAD software (Digistell; Digilea, Montpellier, France). For the specific design, an Akers clasp was selected for #34, a ring clasp for #37, and an RPI clasp for #45 as the abutment, and a lingual bar was set as the major connector.

2.1.2. Fabrication data

Based on the design data, the following three experimental conditions were set using CAM software (CAMbridge; 3shape, Copenhagen, Denmark): 1) a 0° condition, in which the polishing surface was downward and the molding angle was set so that each rest was parallel to the platform; 2) a 45° condition, in which the lingual bar was tilted 45° downward from the 0° condition; and 3) a –45° condition, in which the lingual bar was tilted 45° upward from the 0° condition. The support structure was set to be applied automatically, but no support structure was applied to the tissue surface of the lingual bar and the surface in contact with the abutment teeth, considering the decrease in trueness. In addition, the RPD frameworks were placed on a single platform for each condition, and they were arranged on the platform from the side closest to the recoater, which is the mechanism that evenly spreads the metal powder from the metal powder dispenser to the platform (**Fig. 2**). Then, 10 frameworks were fabricated using an SLM machine (EOSINT M270; EOS, Krailling, Germany) under each condition. The machine settings are presented in **Table 1**. Cobalt–chromium (Co–Cr) alloy powder (SP2; EOS, Krailling, Germany) was used as the metal powder (metal material for dental metal–ceramic restoration 222 AFBZX00088000); the details are shown in **Table 2**.

Following the manufacturer's recommendations, the molded framework was annealed at 1000 °C for 30 min, and then shot peened with ceramic particles under a pressure of 3.0 bar. The framework was then homogenized at 1150 °C for 30 min and then removed from the platform along with the support structure using a band saw (DCR240; Ryowa, Tokyo, Japan). The surface of the completed framework was evenly coated with alumina powder (Pure scan powder; Quest Dental, California, USA) with an average particle size of approximately 0.5 μm (auxiliary material for optical impression 227 AFBZX00091000) using a special brush and fixed on a rotating table for scanning; then, 3D data (fabrication data) were captured using a

Table 1. The selective laser melting (SLM) settings used in this study

Yb-fiber laser	195 W
Scan interval	90 μm
Scan speed	1200 mm/s
Laser spot size	100 μm
Layer thickness	20 μm

Table 2. Information on the cobalt-chromium (Co-Cr) alloy powder used in this study

Particle size of the powder		25 μm
Proportions of the components	Co	63.8%
	Cr	24.7%
	Mo	5.1%
	W	5.4%
	Si	1.0%
Physical properties	Liquid phase point	1440 °C
	Solid phase point	1380 °C
	Young's modulus*	210 Gpa
	Proof stress*	690 Mpa
	elongation*	15%

*=Properties of Co-Cr alloy after SLM

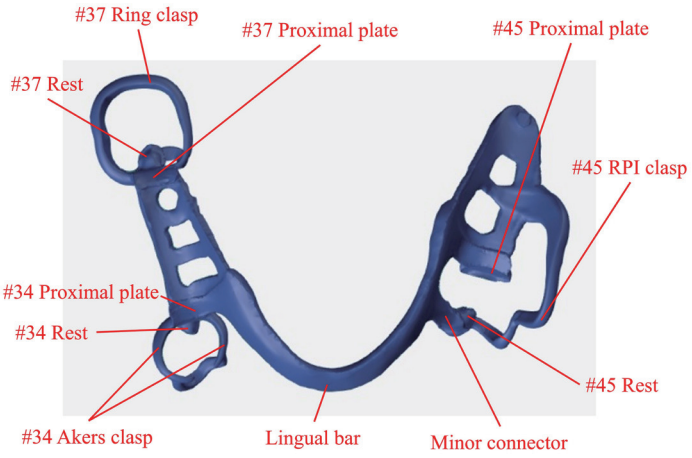

Fig. 3. Measurement site. Rest (#34 Rest, #37 Rest, and #45 Rest), Proximal plate (#34 Proximal plate, #37 Proximal plate, and #45 Proximal plate), Lingual bar, Minor connector, Clasp (#34 Akers clasp, #37 Ring clasp, and #45 RPI clasp).

Fig. 4. Setting of support structures using CAM software (view from above). Left: 0°, center: 45°, right: –45°.

3D scanner (ATOS core200; GOM, Braunschweig, Germany). The table was rotated 360° clockwise and scanned every 45° with the tilt fixed at 0°, 22.5°, 45°, 52.5°, and 60°.

2.2. Calculation of shape error

Regarding the verification method for the shape error, a best-fit algorithm was first used to superimpose the design data with the fabrication data using 3D data inspection software (GOM Inspect, GOM, Braunschweig, Germany). In this study, the local best-fit algorithm, which targets the point set at the center of the fitting surface of the three rests in the RPD framework, was used. A total of 22 verification sites were set at the rest, the proximal plate, the lingual bar (center, intermediate side, and free-end side), the minor connector, and the inner surface of the clasp arm (tip, center, and shoulder of the clasp arm) (**Fig. 3**). Five arbitrary points were set at intervals of approximately 0.5 mm for each verification site, the shape error between the design and fabrication data was calculated for each point, and the average value of the five points was used as the representative value for each verification site.

2.3. Measurement of the number of support structures

The number of support structures was measured by first selecting one representative framework for each condition and then conducting measurements using images from the CAM software (**Fig. 4**). The blue dots in **Figure 4** show the support structures attached to the framework for each condition.

2.4. Analysis of the alloy microstructure

2.4.1. Verification of internal defects by micro-computed tomography (μCT)

To examine the internal defects of each sample, μCT imaging was performed using an inspection CT system (XT H 225 ST; Nikon, Tokyo, Japan) for void analysis. Special software (MyVGL; Volume Graphics, Heidelberg, Germany) was used for the analysis, in which the number of voids in the entire framework was measured for each sample. In addition, the framework was classified into two groups: large components (lingual bar and retention grid) and small components (rests, proximal plates, clasps, and minor connector); the number of voids in each of the two groups was measured for each sample.

2.4.2. Measurement of surface roughness

The surface roughness of the center of the lingual bar was measured using a laser microscope (OLS4000; Olympus, Tokyo, Japan). The arithmetical mean height (Sa) was used as the evaluation parameter. The measurement magnification was set at 20×, and each sample was fixed so that the tissue surface of the lingual bar was perpendicular to the long axis of the lens of the laser microscope. Five arbitrary points were set at intervals of approximately 0.5 mm for each verification site. The average value of the five points was used as the representative value for the sample.

2.5. Statistical analysis

The Kruskal–Wallis test was used to compare the obtained shape error, total number of internal defects, total defect volume, and surface roughness for the various molding conditions. Bonferroni correction was used for subsequent multiple comparisons.

In addition, for internal defects, Wilcoxon's signed rank test was used to compare the number of defects and defect volume between

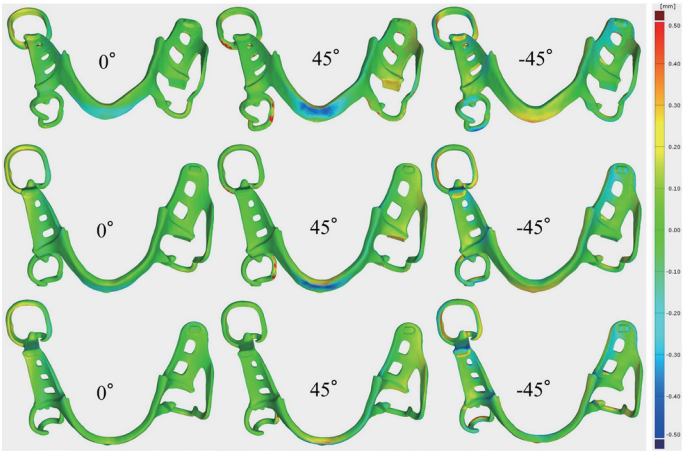

Fig. 5. Color map of shape error (upper: view from forward, middle: view from above, lower: view from backward). Left: 0°, center: 45°, right: −45°.

the large and small components for each molding condition.

All analyses were performed using SPSS statistical software (version 25; IBM, New York, USA), with the significance level set at 0.05.

3. Results

3.1. Comparison of shape error

The shape error for all measurement sites ranged from −0.14 to 0.14 mm at 0° (median: 0.01 mm), from −0.24 to 0.25 mm at 45° (median: 0.02 mm), and from −0.27 to 0.20 mm at −45° (median: 0.02 mm) (**Fig. 5**). The results for each validation site are presented below:

3.1.1. Rests

Regarding the rest, all of the points displaced the fabrication data in the positive direction, which is the direction in which the fabrication data approach the model, compared with the design data (**Table 3**). The #34 rest showed no statistically significant differences between any of the molding angles. The #37 rest showed the smallest displacement, at −45°, with statistically significant differences between 45° and 0° and between 45° and −45°. The #45 rest showed the smallest displacement at 0°, and a statistically significant difference between 0° and −45°, but no statistically significant difference between the other conditions.

3.1.2. Proximal plates

With respect to the proximal plate, except for #34 and #45 in the 0° and 45° conditions, the fabrication data were displaced in the negative direction, the direction away from the model, compared with the design data (**Table 3**). The #34 and #37 proximal plates showed the smallest displacements at 0° and 45°, respectively, and statistically significant differences were observed between −45° and 0° and between −45° and 45°. The #45 proximal plate showed the smallest displacement at 0°, and a statistically significant difference was observed between all conditions.

3.1.3. Connectors

The minor connector showed negative displacement in all conditions, with a smaller displacement at −45°, 0°, and 45°, in that order (**Table 3**). A statistically significant difference was found between 45° and −45°.

The major connector exhibited a large displacement at the center of the lingual bar. In the 0° and 45° conditions, the displacement of the fabricated data was in the negative direction, in which the fabricated data moved away from the model in relation to the design data, and the displacement at 45° was approximately twice as large as that at 0°. Moreover, −45° exhibited positive displacement. Statistically significant differences were observed between all conditions.

Both the free-end and intermediate sides showed negative displacement in all conditions, with the smallest negative displacement at 0°, followed by 45° and −45°. Statistically significant differences were observed between −45° and 0° and between −45° and 45° on the intermediate side. On the free-end side, statistically significant differences were found only between 0° and −45°.

3.1.4. Clasps

The #34 clasp showed displacement in the negative direction at −45° and in the positive direction at 0° and 45° at all points of the buccal-side arm. In particular, pronounced negative displacements were observed at the tip and shoulder regions of −45° (**Table 4**). No statistically significant difference was found between 0° and 45°, but a statistically significant difference was seen between −45° and the other two conditions for all clasps.

In contrast, the lingual arm showed negative displacement at the tips of 45° and −45° and at the shoulder of −45° (**Table 4**). In contrast, all other sites showed positive displacement, regardless of the condition. The displacement tended to increase in the order of the tip, center, and shoulder. A statistically significant difference was observed between 0° and −45° for the tip, and between 0° and −45° and between 45° and −45° for the shoulder. No statistically significant difference was observed in the center between any of the conditions.

In #37, the tip showed negative displacement under all conditions, while the center and shoulder showed positive displacement (**Table 4**). The smallest displacement was observed at the tip at 0°, and a statistically significant difference was observed between −45° and the other two conditions. In the center, the smallest displacement was observed at −45°, and a statistically significant difference was observed between 0° and the other two conditions. In the shoulder region, 45° showed the smallest displacement, and a statistically significant difference was observed between 45° and −45°.

In #45, the tip of the clasp at 0° and the tip and center of the clasp at 45° showed displacement in the negative direction, whereas the rest showed displacement in the positive direction (**Table 4**). Moreover, −45° showed a large positive displacement, regardless of the location of the tip, center, and shoulder of the clasp arm. Statistically significant differences were observed between −45° and the other two conditions for the tip, and between 45° and the other two conditions for the center. No statistically significant differences were found in the shoulder region between any of the conditions.

Table 3. Median and interquartile range value of the occlusal rest, proximal plate and connector (mm)

						P value	Adjusted P value		
			0°	45°	-45°	Group	0°vs45°	0°vs-45°	45°vs-45°
Rest	#34	Median	0.039	0.028	0.035	0.612			
		Min	-0.023	0.014	-0.026				
		Max	0.094	0.069	0.044				
		IQR	0.055	0.021	0.033				
	#37	Median	0.036	0.078	0.033	**0.001	**0.004	1.000	**0.004
		Min	-0.022	0.035	0.022				
		Max	0.072	0.095	0.066				
		IQR	0.015	0.010	0.024				
	#45	Median	0.009	0.048	0.066	**0.009	0.402	**0.006	0.346
		Min	-0.060	-0.060	0.019				
		Max	0.060	0.096	0.116				
		IQR	0.045	0.069	0.042				
Proximal plate	#34	Median	0.024	0.060	-0.189	**0.000	0.099	*0.018	**0.000
		Min	-0.006	0.036	-0.233				
		Max	0.052	0.091	-0.168				
		IQR	0.022	0.018	0.019				
	#37	Median	-0.077	-0.072	-0.145	**0.000	1.000	**0.002	**0.000
		Min	-0.115	-0.072	-0.191				
		Max	-0.056	-0.050	-0.122				
		IQR	0.019	0.021	0.027				
	#45	Median	0.012	0.225	-0.128	**0.000	*0.033	*0.033	**0.000
		Min	0.002	0.175	-0.186				
		Max	0.040	0.251	-0.060				
		IQR	0.017	0.018	0.060				
connector	Minor connector	Median	-0.055	-0.070	-0.037	**0.009	0.239	0.586	**0.007
		Min	-0.069	-0.114	-0.067				
		Max	-0.043	-0.038	-0.014				
		IQR	0.011	0.034	0.035				
	Lingual bar Center	Median	-0.122	-0.209	0.135	**0.000	*0.033	*0.033	**0.000
		Min	-0.136	-0.238	0.092				
		Max	-0.092	-0.153	0.159				
		IQR	0.012	0.013	0.020				
	Lingual bar Left-side Joining area (Intermediate)	Median	-0.029	-0.054	-0.099	**0.000	0.112	**0.000	*0.017
		Min	-0.061	-0.069	-0.145				
		Max	-0.006	-0.037	-0.083				
		IQR	0.009	0.006	0.027				
	Lingual bar Right-side Joining area (Free-end)	Median	-0.032	-0.050	-0.081	**0.000	0.281	**0.000	0.055
		Min	-0.050	-0.021	-0.050				
		Max	-0.019	-0.021	-0.048				
		IQR	0.013	0.032	0.020				

IQR=interquartile range
**=significant difference at p<0.01
*=significant difference at p<0.05

3.2. Numbers of support structures

The numbers of support structures attached under each condition were 632 at 0°, 471 at 45°, and 436 at −45°.

3.3. Internal defects

A typical image of the internal defects is shown in **Figure 6**. The total number of defects ranged from 0 to 11 (median: 1) at 0°, 0 to 43 (median: 2) at 45°, and 0 to 16 (median: 2) at −45°. The total defect volume ranged from 0.000 to 0.018 mm^3 (median: 0.000 mm^3) at 0°, 0.000 to 0.059 mm^3 (median: 0.004 mm^3) at 45°, and 0.000 to 0.030 mm^3 (median: 0.003 mm^3) at −45°. No statistically significant difference was found with respect to the total number of defects or total defect volume among the molding angles (**Table 5**).

Then, the framework was classified into large and small components and investigated for each angle condition. For 0°, the number of defects ranged from 0 to 11 (median: 0) regarding the large components and from 0 to 1 (median: 0) regarding the small components

Table 4. Median and interquartile range value of the clasps (mm)

							P value	Adjusted P value		
				0°	45°	-45°	Group	0°vs45°	0°vs-45°	45°vs-45°
Akers clasp	Buccal arm	Tip	Median	0.031	0.022	-0.170	**0.000	1.000	**0.000	**0.001
			Min	0.000	-0.038	-0.211				
			Max	0.060	0.068	-0.153				
			IQR	0.026	0.034	0.026				
		Center	Median	0.039	0.049	-0.030	**0.001	1.000	*0.011	**0.001
			Min	-0.004	-0.022	-0.101				
			Max	0.052	0.081	0.015				
			IQR	0.037	0.026	0.061				
		Shoulder	Median	0.048	0.031	-0.224	**0.000	1.000	**0.000	**0.002
			Min	0.013	0.017	-0.267				
			Max	0.081	0.059	-0.212				
			IQR	0.040	0.022	0.017				
	Lingual arm	Tip	Median	0.014	-0.009	-0.040	**0.007	0.824	**0.006	0.134
			Min	-0.026	-0.035	-0.060				
			Max	0.044	0.036	0.013				
			IQR	0.017	0.050	0.037				
		Center	Median	0.035	0.045	0.056	0.191			
			Min	0.007	0.004	0.023				
			Max	0.066	0.091	0.134				
			IQR	0.020	0.037	0.059				
		Shoulder	Median	0.053	0.067	-0.113	**0.000	1.000	**0.001	**0.000
			Min	0.026	0.022	-0.159				
			Max	0.095	0.105	-0.094				
			IQR	0.021	0.021	0.026				
Ring clasp		Tip	Median	-0.013	-0.034	-0.143	**0.000	0.759	**0.000	*0.018
			Min	-0.058	-0.087	-0.255				
			Max	0.005	0.000	-0.012				
			IQR	0.024	0.034	0.049				
		Center	Median	0.126	0.069	0.050	**0.000	**0.003	**0.000	1.000
			Min	0.099	0.033	-0.075				
			Max	0.137	0.117	0.091				
			IQR	0.009	0.019	0.032				
		Shoulder	Median	0.041	0.003	0.084	**0.000	0.060	0.058	**0.000
			Min	0.013	-0.052	0.044				
			Max	0.064	0.109	0.127				
			IQR	0.019	0.013	0.032				
RPI clasp		Tip	Median	-0.012	-0.047	0.142	**0.000	0.281	**0.009	**0.000
			Min	-0.058	-0.114	0.045				
			Max	-0.002	-0.014	0.200				
			IQR	0.023	0.014	0.084				
		Center	Median	0.032	-0.023	0.099	**0.000	*0.027	0.062	**0.000
			Min	0.014	-0.079	0.067				
			Max	0.097	0.018	0.129				
			IQR	0.031	0.032	0.029				
		Shoulder	Median	0.020	0.055	0.079	0.131			
			Min	-0.015	0.008	0.051				
			Max	0.095	0.119	0.106				
			IQR	0.088	0.073	0.032				

IQR=interquartile range
**=significant difference at p<0.01
*=significant difference at p<0.05

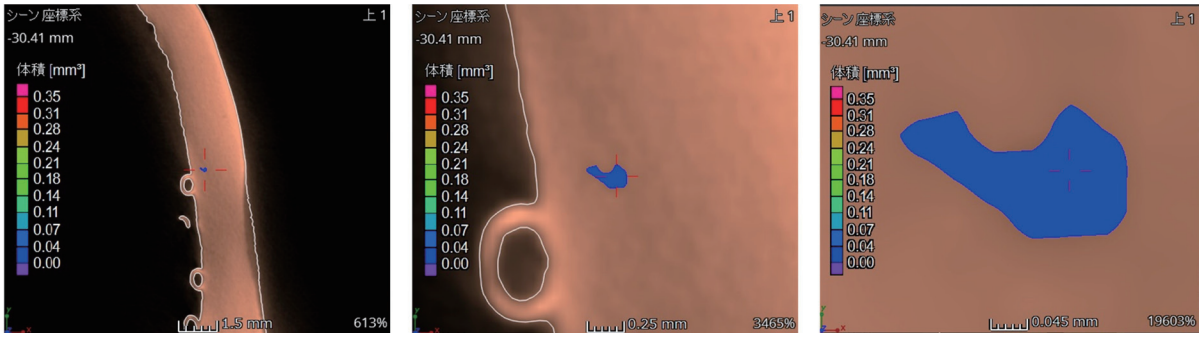

Fig. 6. An example of the image of internal defects of the selective laser melting (SLM) framework. Left: low magnification, center: middle magnification, right: high magnification.

Table 5. Median and interquartile range values for the overall internal defetcs (number and volume)

Internal defects					P value	Adjusted P value		
		0°	45°	-45°	Group	0°vs45°	0°vs-45°	45°vs-45°
Number	Median	1	2	2	0.686			
	Min	0	0	0				
	Max	11	43	16				
	IQR	4.80	8.25	4.50				
Volume (mm^3)	Median	0.000	0.004	0.003	0.665			
	Min	0.000	0.000	0.000				
	Max	0.018	0.059	0.030				
	IQR	0.008	0.025	0.008				

IQR=interquartile range

(**Table 6**). The defect volume ranged from 0.000 to 0.018 mm^3 (median: 0.000 mm^3) with respect to the large components and from 0.000 to 0.000 mm^3 (median: 0.000 mm^3) with respect to the small components (**Table 6**). No statistically significant difference was found regarding the number of defects or defect volume between the large and small components.

At 45°, the number of defects ranged from 0 to 34 (median: 2) regarding the large components and from 0 to 9 (median: 0) regarding the small components (**Table 6**). The defect volume ranged from 0.000 to 0.046 mm^3 (median: 0.004 mm^3) with respect to the large components and from 0.000 to 0.013 mm^3 (median: 0.000 mm^3) with respect to the small components (**Table 6**). A statistically significant difference was observed regarding the number of defects and defect volume between the large and small components.

At −45°, the number of defects ranged from 0 to 12 (median: 1) regarding the large components and from 0 to 4 (median: 0) regarding the small components (**Table 6**). The defect volume ranged from 0.000 to 0.022 mm^3 (median: 0.003 mm^3) with respect to the large components and from 0.000 to 0.008 mm^3 (median: 0.000 mm^3) with respect to the small components (**Table 6**). A statistically significant difference was observed regarding the number of defects and defect volume between the large and small components.

3.4. Surface roughness

A typical image of the roughness of the tissue surface by angle for the center of the lingual bar is shown in **Figure 7**. The surface roughness ranged from 1.31 to 2.76 μm (median: 1.80 μm) at 0°, 1.73 to 3.92 μm (median: 2.51 μm) at 45°, and 1.10 to 1.75 μm (median:

Table 6. Median and interquartile range values for the internal defects at each angle (number and volume)

Internal defects			Major part	Minor part	P value
Number	0°	Median	0	0	0.102
		Min	0	0	
		Max	11	1	
		IQR	4.8	0	
	45°	Median	2	0	***0.028**
		Min	0	0	
		Max	34	9	
		IQR	7.5	0	
	-45°	Median	1	0	***0.043**
		Min	0	0	
		Max	12	4	
		IQR	3.75	0.75	
Volume (mm^3)	0°	Median	0.000	0.000	0.068
		Min	0.000	0.000	
		Max	0.018	0.000	
		IQR	0.008	0.000	
	45°	Median	0.004	0.000	***0.043**
		Min	0.000	0.000	
		Max	0.046	0.013	
		IQR	0.025	0.000	
	-45°	Median	0.003	0.000	***0.043**
		Min	0.000	0.000	
		Max	0.022	0.008	
		IQR	0.008	0.001	

IQR=interquartile range
*=significant difference at $p<0.05$

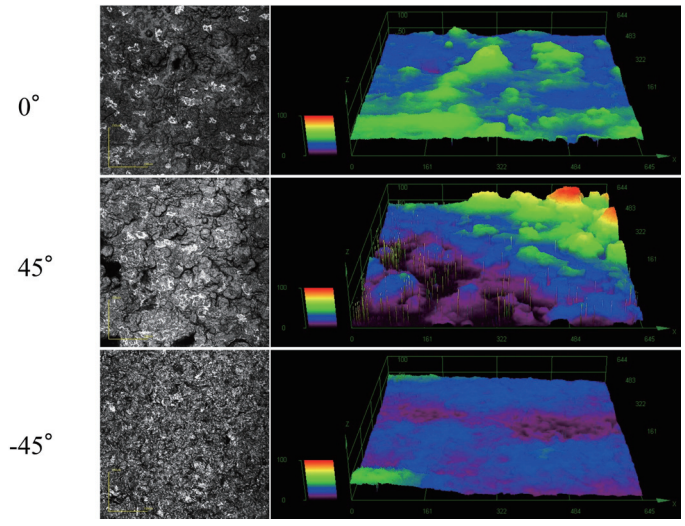

Fig. 7. Color map of surface roughness (view from the tissue surface of the center of the lingual bar). Left: 0°, center: 45°, right: −45°.

1.31 μm) at −45° (**Table 7**). A statistically significant difference was observed between 45° and −45°, but no statistically significant difference was observed between any of the other conditions.

4. Discussion

4.1. Significance of this study

In previous studies, the trueness of RPD components was evaluated by fabricating only the retainer[27] or by fabricating dumbbell-shaped specimens to evaluate the microstructure and surface roughness[21]. In the present study, we fabricated an RPD framework using SLM and evaluated the shape error of each component, which is a substantial difference from previous studies. Therefore, we were able to evaluate the deviation of the shape error caused by the simultaneous connection of each component at the same time.

Compared with the digital technique to verify the fit between STL data and fabrication data, the analog technique is considered to be useful in verifying the fit between the actual framework and the model. However, to evaluate the shape error, most previous studies used analog technology with a silicone replica of the framework, which has the disadvantage of being error-prone[28]. The method using silicon replicas is affected by both the framework and model fabrication errors. Therefore, this study takes advantage of digital technology because all frameworks should be comparable in a single STL data, inter-technician errors caused by adjustment and polishing can be eliminated, and the three rest points, which are the most important for the RPD framework to fit, are targeted by the local best-fit algorithm, thus reducing the problems of alignment. In the present study, we applied digital technology to almost all processes, from the fabrication of the metal framework as a sample to the fitness evaluation and verification of the microstructure; therefore, the possibility of errors in the fabrication and evaluation therein is extremely small[29].

As for internal defects, a previous study[22] compared Co–Cr clasps fabricated using the conventional casting method with those fabricated by SLM. Regarding surface roughness, another study[30] compared titanium clasps fabricated by a casting technique with those fabricated by SLM. However, to our knowledge, this is the first study to compare the internal defects and surface roughness of the framework itself. Therefore, compared with previous studies, the present study was able to evaluate trueness quantitatively, thereby ensuring objectivity.

4.2. Discussion of the results

The trueness of the RPD framework fabricated by SLM was excellent, with a shape error of 0° for all measurement sites and a smaller range compared with the other conditions. This is thought to occur because the number of support structures attached differed depending on the SLM molding angle, and the number of support structures attached was higher at 0° (**Fig. 4**). It has been reported that the design of the support structure has a strong influence on fabrication using SLM[31], which suggests the necessity of arranging the product so that the number of support structure attachments is not extremely low. More attention is required when the setting range of the support structure is extremely limited in the part of the framework where the trueness on the fitting surface side is important, as the cutting of the support structure can significantly impair the quality[32]. As mentioned above, there is an issue in that the automatic support setting of CAM software sets the support structures on the fitting surface of RPD frameworks, and it is not possible to set the support structures 100% automatically; this is worthy of future study.

Looking at the shape error of each component of the framework in detail, for the rests, the shape errors were large at 45° for #37 and at −45° for #45, but both rests were set at a higher position relative to the platform. As for the proximal plate, the shape error was large at −45° for #34, which was also set at a higher position. This suggests that the set position of the platform could affect trueness. Tasaka et al.[27] reported that the median shape error of the rest of Akers clasps fabricated by SLM was -0.006 mm (mean, -0.003; SD, 0.001). In comparison, the shape error of the present study was larger, with a median of 0.028-0.039 mm for each condition. Therefore, even if the shape error of each element is small in a framework in which all elements are connected, they may affect each other, resulting in a larger shape error.

Furthermore, for the proximal plate, the shape errors were large at −45° for #37 and at 45° for #45. It is clear that the relationship between the positions of the structures should be considered when molding[33,34]. In this study, no support structure was applied to the tissue surface of the lingual bar and the surface in contact with the abutment teeth, considering the decrease in trueness when the support structure was removed. For example, in the cases of the #37 proximal plate at −45°, #45 proximal plate at −45°, and #34 proximal plate at 45°, the support structure was not set using the CAM software before SLM. Therefore, the shape error tended to be larger in this region, where an overhang was observed. It has been reported that deformation tends to occur in overhanging regions without a support structure[35], and as the width and thickness of the overhanging region increase, so does the deformation[36]. Therefore, the attachment of the support structure is considered a factor that greatly affects trueness.

Regardless of the molding angle, the center of the lingual bar showed a large local error. The error was especially large at 45°, and the support structure was placed vertically from the platform side in

Table 7. Median and interquartile range values for the surface roughness (Sa)

Surface roughness					P value	Adjusted P value		
		0°	45°	-45°	Group	0°vs45°	0°vs-45°	45°vs-45°
Lingual bar (Center)	Median	1.797	2.514	1.310	**0.000	0.105	0.058	**0.000
	Min	1.307	1.727	1.103				
	Max	2.759	3.923	1.754				
	IQR	0.369	0.546	0.113				

IQR=interquartile range
**=significant difference at p<0.01

only one row on the upper edge of the lingual bar polishing surface. Conversely, at 0° and −45°, the support structure at the center of the lingual bar was evenly placed in three or more rows on the polishing surface of the lingual bar, resulting in a smaller error than that at 45°. This result suggests that the setting of the support structure is closely related to the trueness of the SLM. In addition, the fact that the displacements at 0° and −45° were opposite to each other suggests the possibility that the displacements were caused by the difference in the height of the object relative to the platform.

For #34, the number of support structures to the tip, center, and shoulder of the clasp of the buccal arm were extremely small at −45° compared with the other conditions, and the difference value was also large. In the lingual arm, the numbers of support structures were similar in all three conditions, except for the shoulder of the clasp, and the range of the error was also similar. These results suggest that the number of support structures is significant, even for small components. For #45, the number of support structures was almost equal, regardless of the molding angle, but a large difference in trueness was observed among the molding angles in the central part of the clasp. At −45°, the center of the clasp was formed at approximately 90° with respect to the support structure, and deformation resulting from metal shrinkage occurred within the expected range. However, at 0° and −45°, the center part was positioned at an angle to the platform, and the direction of the metal shrinkage was also inclined, resulting in unexpected deformation. These results suggest that it is necessary to increase the support structure attachment manually when setting the support structure to avoid deformation of components that are expected to be deformed.

In this study, no difference was observed in the total number of internal defects and the total volume for each molding angle. However, when the results were compared between relatively thick and large components, such as a lingual bar and a retention grid, and relatively small components, no difference was observed in the occurrence of internal defects at 0°, but many internal defects were observed in the large components at 45° and −45°. This finding suggests that the molding angle did not affect the small components in terms of the development of internal defects, but did affect the large components, especially the major connecter.

Regarding the center of the lingual bar, the roughness of the tissue surface was the smallest at −45° and its irregularities were evenly distributed, whereas the surface roughness was the largest at 45°. The center of the lingual bar was closest to parallel to the platform at −45°, while it was placed diagonally at 45°, suggesting that the roughness was superior for surfaces that were closer to parallel to the platform. These findings suggest that part of the surface of the molding produced by SLM that directly contacts the tooth surface or oral mucosa should be placed parallel to the platform as much as possible. Because Tasaka et al.[7] reported a large local error in the center of the lingual bar of the SLM framework, that area was chosen as the region of interest for surface roughness in this study. Surface roughness is also a factor in the adhesion of denture plaque, and the area in contact with the mucosa is a risk factor for denture stomatitis.

In this study, it was possible to control the occurrence of internal defects to some extent by changing the molding angle, but it was difficult to control the local displacement of the lingual bar. Local displacements can concentrate residual stresses, leading to a decrease in strength. In recent years, hybrid processing that combines SLM and milling technologies has become possible[20,23], so the displacement can be improved by modifying the data before SLM is performed in areas where large deformations are expected beforehand, and by milling the compensation for trueness after the formation. It is also possible to make the molding surface smoother, which should be explored in future research.

In addition, considering that different thermal stresses in the center and periphery of the platform affect the shape of the final product, the output of each group was printed separately on each platform. In the machine used in this study, the maximum number of frameworks that could be fabricated was 15, which was the same regardless of the angle. The molding times for one or 15 frameworks at 0°, 45°, and −45° were 4.0 h and 16.5 h, 5.6 h and 19.5 h, and 5.5 h and 20.8 h, respectively. Therefore, from the viewpoint of work time efficiency, 0° is the best way to manufacture the framework with the SLM machine used in this study.

4.3. Limitations and future prospects

In this study, we verified the trueness of the framework with respect to differences in the SLM molding angle; however, we did not conduct a comparison with frameworks fabricated by the conventional casting method. To achieve this, it will be necessary to consider a method to separate only the data of the wax part from the wax-up completed on the refractory model, which is the conventional method[37]. Considering the design of RPD frameworks, there is a wide range of variations in the number of missing teeth, missing sites, and different forms of major connectors. Because the simulation model used in this study is only one example, it does not apply to all frameworks; thus, further studies are needed.

5. Conclusion

The results of this study revealed that the trueness of the RPD framework and defects, such as the expression of internal defects and surface roughness, were affected by the difference in the SLM molding angle.

Acknowledgments

This work was partially supported by the Tokai University Imaging Center for Advanced Research.

Conflicts of interest

There are no conflicts of interest to declare in regard to this study.

References

[1] Sulaiman TA. Materials in digital dentistry—A review. J Esthet Restor Dent. 2020;32:171–81. https://doi.org/10.1111/jerd.12566, PMID:31943720

[2] Fang C, An J, Bruno A, Cai X, Fan J, Fujimoto J, *et al.* Consensus recommendations of three-dimensional visualization for diagnosis and management of liver diseases. Hepatol Int. 2020;14:437–53. https://doi.org/10.1007/s12072-020-10052-y, PMID:32638296

[3] Arafa KAO. Assessment of the fit of removable partial denture fabricated by computer-aided designing/computer aided manufacturing technology. Saudi Med J. 2018;39:17–22. https://doi.org/10.15537/smj.2018.1.20796, PMID:29332104

[4] Kalberer N, Mehl A, Schimmel M, Müller F, Srinivasan M. CAD-CAM milled versus rapidly prototyped (3D-printed) complete dentures: an in vitro evaluation of trueness. J Prosthet Dent. 2019;121:637–43. https://doi.org/10.1016/j.prosdent.2018.09.001, PMID:30711292

[5] Tasaka A, Matsunaga S, Odaka K, Ishizaki K, Ueda T, Abe S, *et al.* Accuracy and retention of denture base fabricated by heat curing and additive manufacturing. J Prosthodont Res. 2019;63:85–9. https://doi.org/10.1016/j.jpor.2018.08.007, PMID:30584053

[6] Lee C, Kobayashi H, Lee SR, Ohyama H. The Role of Digital 3D Scanned Models in Dental Students' Self-Assessments in Preclinical Operative Dentistry. J Dent Educ. 2018;82:399–405. https://doi.org/10.21815/JDE.018.046, PMID:29606657

[7] Tasaka A, Shimizu T, Kato Y, Okano H, Ida Y, Higuchi S, *et al.* Accuracy of removable partial denture framework fabricated by casting with a 3D printed pattern and selective laser sintering. J Prosthodont Res. 2020;64:224–30. https://doi.org/10.1016/j.jpor.2019.07.009, PMID:31466919

[8] Carneiro Pereira AL, Bezerra de Medeiros AK, de Sousa Santos K, Oliveira de Almeida É, Seabra Barbosa GA, da Fonte Porto Carreiro A. Accuracy of CAD-CAM systems for removable partial denture framework fabrication: A systematic review. J Prosthet Dent. 2021;125:241–8. https://doi.org/10.1016/j.prosdent.2020.01.003, PMID:32147252

[9] Arnold C, Hey J, Schweyen R, Setz JM. Accuracy of CAD-CAM-fabricated removable partial dentures. J Prosthet Dent. 2018;119:586–92. https://doi.org/10.1016/j.prosdent.2017.04.017, PMID:28709674

[10] Lima JMC, Anami LC, Araujo RM, Pavanelli CA. Removable partial dentures: use of rapid prototyping. J Prosthodont. 2014;23:588–91. https://doi.org/10.1111/jopr.12154, PMID:24750472

[11] Soltanzadeh P, Suprono MS, Kattadiyil MT, Goodacre C, Gregorius W. An In Vitro Investigation of Accuracy and Fit of Conventional and CAD/CAM Removable Partial Denture Frameworks. J Prosthodont. 2019;28:547–55. https://doi.org/10.1111/jopr.12997, PMID:30407685

[12] Alageel O, Abdallah MN, Alsheghri A, Song J, Caron E, Tamimi F. Removable partial denture alloys processed by laser-sintering technique. J Biomed Mater Res B Appl Biomater. 2018;106:1174–85. https://doi.org/10.1002/jbm.b.33929, PMID:28561993

[13] Peng PW, Hsu CY, Huang HY, Chao JC, Lee WF. Trueness of removable partial denture frameworks additively manufactured with selective laser melting. J Prosthet Dent. 2020;S0022-3913(20)30558-8. https://doi.org/10.1016/j.prosdent.2020.06.035, PMID:33223197

[14] Alharbi N, Wismeijer D, Osman R. Additive Manufacturing Techniques in Prosthodontics: Where Do We Currently Stand? A Critical Review. Int J Prosthodont. 2017;30:474–84. https://doi.org/10.11607/ijp.5079, PMID:28750105

[15] Takaichi A, Fueki K, Murakami N, Ueno T, Inamochi Y, Wada J, *et al.* A systematic review of digital removable partial dentures. Part II: CAD/CAM framework, artificial teeth, and denture base. Journal of Prosthodontic Research 2021;advpub. https://doi.org/10.2186/jpr.JPR_D_20_00117.

[16] Al Mortadi N, Alzoubi KH, Williams R. A Scoping Review on the Accuracy of Fit of Removable Partial Dentures in a Developing Digital Context. Clin Cosmet Investig Dent. 2020;12:551–62. https://doi.org/10.2147/CCIDE.S282300, PMID:33244275

[17] Steinmassl O, Dumfahrt H, Grunert I, Steinmassl PA. CAD/CAM produces dentures with improved fit. Clin Oral Investig. 2018;22:2829–35. https://doi.org/10.1007/s00784-018-2369-2, PMID:29468600

[18] Kanazawa M, Iwaki M, Minakuchi S, Nomura N. Fabrication of titanium alloy frameworks for complete dentures by selective laser melting. J Prosthet Dent. 2014;112:1441–7. https://doi.org/10.1016/j.prosdent.2014.06.017, PMID:25258261

[19] Ni D, Dong Y, Peng JP, Xu Y, Yang MX, Dai YJ. [Effect of different support angles on the fitness of removable partial denture framework fabricated using selective laser melting technique]. Zhonghua Kou Qiang Yi Xue Za Zhi. 2020;55:165–70. https://doi.org/10.3760/cma.j.issn.1002-0098.2020.03.004, PMID:32193912

[20] Nakata T, Shimpo H, Ohkubo C. Clasp fabrication using one-process molding by repeated laser sintering and high-speed milling. J Prosthodont Res. 2017;61:276–82. https://doi.org/10.1016/j.jpor.2016.10.002, PMID:27825561

[21] Kajima Y, Takaichi A, Nakamoto T, Kimura T, Yogo Y, Ashida M, *et al.* Fatigue strength of Co–Cr–Mo alloy clasps prepared by selective laser melting. J Mech Behav Biomed Mater. 2016;59:446–58. https://doi.org/10.1016/j.jmbbm.2016.02.032, PMID:26974490

[22] Schweiger J, Güth J-F, Erdelt K-J, Edelhoff D, Schubert O. Internal porosities, retentive force, and survival of cobalt–chromium alloy clasps fabricated by selective laser-sintering. J Prosthodont Res. 2020;64:210–6. https://doi.org/10.1016/j.jpor.2019.07.006, PMID:31680054

[23] Torii M, Nakata T, Takahashi K, Kawamura N, Shimpo H, Ohkubo C. Fitness and retentive force of cobalt-chromium alloy clasps fabricated with repeated laser sintering and milling. J Prosthodont Res. 2018;62:342–6. https://doi.org/10.1016/j.jpor.2018.01.001, PMID:29428170

[24] Forrester K, Sheridan R, Phoenix RD. Assessing the Accuracy of Casting and Additive Manufacturing Techniques for Fabrication of a Complete Palatal Coverage Metal Framework. J Prosthodont. 2019;28:811–7. https://doi.org/10.1111/jopr.13076, PMID:31115125

[25] Stewart's Clinical Removable Partial Prosthodontics. Fourth Edition n.d. http://www.quintpub.com/display_detail.php3?psku=B4856#.YUNKlrj7Tic.

[26] McCracken's Removable Partial Prosthodontics - 13th Edition n.d. https://www.elsevier.com/books/mccrackens-removable-partial-prosthodontics/carr/978-0-323-33990-2.

[27] Tasaka A, Kato Y, Odaka K, Matsunaga S, Goto T, Abe S, *et al.* Accuracy of Clasps Fabricated with Three Different CAD/CAM Technologies: Casting, Milling, and Selective Laser Sintering. Int J Prosthodont. 2019;32:526–9. https://doi.org/10.11607/ijp.6363, PMID:31664269

[28] Ye H, Ning J, Li M, Niu L, Yang J, Sun Y, *et al.* Preliminary Clinical Application of Removable Partial Denture Frameworks Fabricated Using Computer-Aided Design and Rapid Prototyping Techniques. Int J Prosthodont. 2017;30:348–53. https://doi.org/10.11607/ijp.5270, PMID:28697204

[29] Tregerman I, Renne W, Kelly A, Wilson D. Evaluation of removable partial denture frameworks fabricated using 3 different techniques. J Prosthet Dent. 2019;122:390–5. https://doi.org/10.1016/j.prosdent.2018.10.013, PMID:30948301

[30] Takahashi K, Torii M, Nakata T, Kawamura N, Shimpo H, Ohkubo C. Fitness accuracy and retentive forces of additive manufactured titanium clasp. J Prosthodont Res. 2020;64:468–77. https://doi.org/10.1016/j.jpor.2020.01.001, PMID:32063534

[31] Weber S, Montero J, Bleckmann M, Paetzold K. PARAMETERS ON SUPPORT STRUCTURE DESIGN FOR METAL ADDITIVE MANUFACTURING. Proceedings of the Design Society: DESIGN Conference. 2020;1:1145–54. https://doi.org/10.1017/dsd.2020.14

[32] Jiang J, Xu X, Stringer J. Support Structures for Additive Manufacturing: A Review. Journal of Manufacturing and Materials Processing. 2018;2:64. https://doi.org/10.3390/jmmp2040064

[33] Bruyneel M, Duysinx P. Note on topology optimization of continuum structures including self-weight. Struct Multidiscipl Optim. 2005;29:245–56. https://doi.org/10.1007/s00158-004-0484-y

[34] Martínez J, Dumas J, Lefebvre S, Wei L-Y. Structure and appearance optimization for controllable shape design. ACM Trans Graph 2015;34:229:1-229:11. https://doi.org/10.1145/2816795.2818101.

[35] Yang L, Ferrucci M, Mertens R, Dewulf W, Yan C, Shi Y, *et al.* An investigation into the effect of gradients on the manufacturing fidelity of triply periodic minimal surface structures with graded density fabricated by selective laser melting. J Mater Process Technol. 2020;275:116367. https://doi.org/10.1016/j.jmatprotec.2019.116367

[36] Ameen W, Al-Ahmari A, Mohammed MK. Self-supporting overhang structures produced by additive manufacturing through electron beam melting. Int J Adv Manuf Technol. 2019;104:2215–32. https://doi.org/10.1007/s00170-019-04007-3

[37] Suzuki Y, Shimizu S, Waki T, Shimpo H, Ohkubo C. Laboratory efficiency of additive manufacturing for removable denture frameworks: A literature-based review. Dent Mater J. 2021;40:265–71. https://doi.org/10.4012/dmj.2020-206, PMID:33361665